

## Research Paper

## Improving Sound Insulation in Low Frequencies by a Three-Component Cladding Acoustic Metamaterial Panel

Na TAN, Xiaowei YAN, Bingfei LIU\*

*Aeronautical Engineering College, Civil Aviation University of China  
Tianjin, China*\*Corresponding Author e-mail: [bingfeiliu2@126.com](mailto:bingfeiliu2@126.com)*(received September 6, 2023; accepted October 28, 2023; published online February 2, 2024)*

In this paper, a three-component cladding acoustic metamaterial panel with good sound insulation effect in the low-frequency range is proposed. The sound transmission loss of metamaterial panels under different structural configurations and different material parameters is investigated by combining finite element simulation calculations with experimental research. The results show that the closer the center of gravity of the scatterer is to the substrate, the better the stability of the resonance unit, the wider the range of effective sound insulation frequencies, and the higher the degree of normalization. The filling rate of the scatterer is maintained at about 0.5 to obtain a better sound insulation effect. At the same time, choosing lower density materials for the substrate and metal materials with high density and high modulus of elasticity for the scatterer can maximally widen the bandgap and allows for low-frequency sound insulation below 600 Hz. This approach improves the low-frequency sound insulation efficiency of acoustic metamaterials. The results provide important explanations and references for a deeper understanding of the sound insulation mechanism and the effects of different parameters on sound insulation.

**Keywords:** acoustics; acoustic metamaterial panels; sound insulation properties; local resonance; low frequency sound insulation.



Copyright © 2024 The Author(s).  
This work is licensed under the Creative Commons Attribution 4.0 International CC BY 4.0  
(<https://creativecommons.org/licenses/by/4.0/>).

## 1. Introduction

The aerospace and automotive industries use acoustic damping and noise reduction devices to reduce low-frequency noise, a subject considered in many studies (JIANG *et al.*, 2021; CHEN *et al.*, 2021; IANNAC *et al.*, 2021; ATMOJO *et al.*, 2021). In these industries, beyond simply enhancing passenger comfort, the advantages also help to minimize errors in precision instruments caused by vibration (ZUO *et al.*, 2016; SONG, 2015).

The composite columnar local resonant unit is a valuable structural form for engineering purposes (ZHAO *et al.*, 2015; LI *et al.*, 2016). In the studies of WEN *et al.* (2005) and (2008), acoustic crystal plates were constructed with a periodic array of columnar local resonant units attached to it. These studies demonstrated the presence of a local resonant bandgap, effectively suppressing the vibration transmission of the acoustic crystal plate. PENNEC *et al.* (2008) designed

and calculated a crystal consisting of a periodic array of cylindrical dots deposited on a thin layer of uniform material, with the number of bandgaps increasing with the height of the cylinders.

UDICH *et al.* (2010; 2011) created an acoustic metamaterial plate using two types of local resonant units: a single-layer rubber column and a composite rubber column. They analyzed how the unit parameters affected the bandgap characteristics. Additionally, they investigated an acoustic metamaterial plate with regularly attached single-layer rubber columns and confirmed the presence of local resonance bandgaps in this structure. HSU (2011) designed an acoustic metamaterial plate with a stepped local resonant unit and a two-dimensional phononic crystal composed of a stepped resonator array. BADREDDINE ASSOUAR and OUDICH (2012), and BADREDDINE *et al.* (2012) conducted a study on the impact of a double-sided arrangement of columnar resonant units on a thin plate. Their findings suggest that this arrangement effectively

broadens the damping frequency band. Also, they designed two-dimensional acoustic crystals utilizing short cut-off plates on both sides.

HSU *et al.* (2013) explored the band gap and waveguide properties of cylindrical acoustic metamaterial plates with a stepped structure. Similarly, YU *et al.* (2013) put forward the idea of two-dimensional phonon crystals composed of stepped resonator arrays. ZHAO *et al.* (2015) examined the vibration isolation properties of a raised phonon crystal sheet in three different structural forms: single-sided single oscillator, single-sided double oscillator, and double-sided single oscillator. Meanwhile, LI *et al.* (2015) designed two-dimensional binary local resonant phonon plates. HE and WEN (2018) studied the sound insulation properties of acoustic metamaterial plates that contained columnar local resonance units. They also explored how the sound insulation properties were affected by different lattice constants.

ZHOU *et al.* (2020) proposed the use of multilayer rubber cylinders and metal cylinders attached to a thin plate. By combining units with different geometrical parameters, the resulting metamaterial demonstrated improved low-frequency sound insulation efficiency. In their respective studies, YANG *et al.* (2020) and ZHOU *et al.* (2021) proposed novel solutions for low-frequency vibration and noise reduction problems in engineering. YANG *et al.* (2020) introduced a two-dimensional conical scatterer phonon crystal plate, while ZHOU *et al.* (2021) designed a double-sided composite resonator structure and demonstrated a hybrid phonon crystal plate through simulations and experiments. NAKAYAMA *et al.* (2021) presented a practical design for sheet acoustic metamaterials that could be potentially used in industrial applications. Their aim was to develop lightweight and compact materials that could effectively insulate against noise generation effects.

Some properties of phononic crystals hold good application prospects, such as exploring acoustic focusing properties and defect state properties of phononic crystals to guide the design of acoustic functional components. QIU and LIU (2006) used phonon crystals to obtain a directional sound source. LIANG *et al.* (2009) developed an acoustic diode model utilizing phonon crystals. Building upon this work, MALDOVAN (2013) further investigated the practical applications of phonon crystals, demonstrating the theoretical and experimental feasibility of using them for acoustic diodes and cloaks. At the same time, programmable smart metamaterials have also emerged (YIN *et al.*, 2022). The use of phononic crystals in designing of automotive, marine, and aircraft structures has also gained traction as phonon crystal research continues to advance (MA *et al.*, 2018; ZHANG *et al.*, 2016a).

Numerous studies highlight the attention given by scholars to the noise control problems in plate structures, resulting in important achievements. How-

ever, the law governing low-frequency sound insulation of cladding acoustic metamaterials (especially below 600 Hz) remains underexplored. However, the influence of low-frequency noise cannot be ignored in practical production and engineering applications. Therefore, the three-component cladding acoustic metamaterial plate structure was selected as the research object in this paper, aiming to explore the law of low-frequency wideband sound insulation by changing the structural and material parameters of the metamaterial plate. The paper is organized as follows: Sec. 1 provides the introduction, Sec. 2 presents the models and research methods, and Sec. 3 shows the results and discussion. Finally, conclusions are given in Sec. 4.

## 2. Models and methods

### 2.1. Experimental methods

The material chosen for the cladding in the experiments is the methyl vinyl polymer (VMQ) silicone rubber, the substrate material is epoxy resin, and the scatterer material is aluminum. The relevant properties of the materials are given in Table 1. The connection between the epoxy resin plate and the rubber, as well as that between the rubber and the cladding, were realized by superglue with a tight fit. In order to facilitate experimental tests with the ZK1030 circular impedance tube, the plate-type acoustic metamaterial was designed as a circular sample (Figs. 1a and 1b) during the preparation of the acoustic isolation test samples. The circular sample is 100 mm in diameter and contains seven hexagonal acoustic metamaterial cells. The thickness of the substrate is  $e = 1$  mm, the single-cell lattice constant  $a = 30$  mm, and the radius and height of the cladding layer remain unchanged at  $R = 6$  mm and  $H = 9$  mm, respectively. For comparative experiments, the radius of the scatterer is selected to be  $r_1 = 4$  mm and  $r_2 = 5$  mm. The corresponding heights of the scatterer are  $h_1 = 4.75$  mm and  $h_2 = 4.32$  mm, respectively.

Table 1. Material constants of the components.

Materials	Mass density [kg/m <sup>3</sup> ]	Young's modulus [Pa]	Poisson's ratio
Tungsten	19 100	$3.54 \times 10^{11}$	0.35
Lead	11 600	$4.08 \times 10^{10}$	0.42
Copper	8960	$1.1 \times 10^{11}$	0.35
Steel	7780	$2.1 \times 10^{11}$	0.30
Aluminum	2700	$7 \times 10^{10}$	0.33
Epoxy resin	1180	$4.35 \times 10^9$	0.38
Silicone rubber	1300	$1.37 \times 10^5$	0.47

This experiment uses the ZK1030 impedance tube test system, which includes the B&K-23750 power amplifier, Type-3160-A-042 data acquisition instrument,

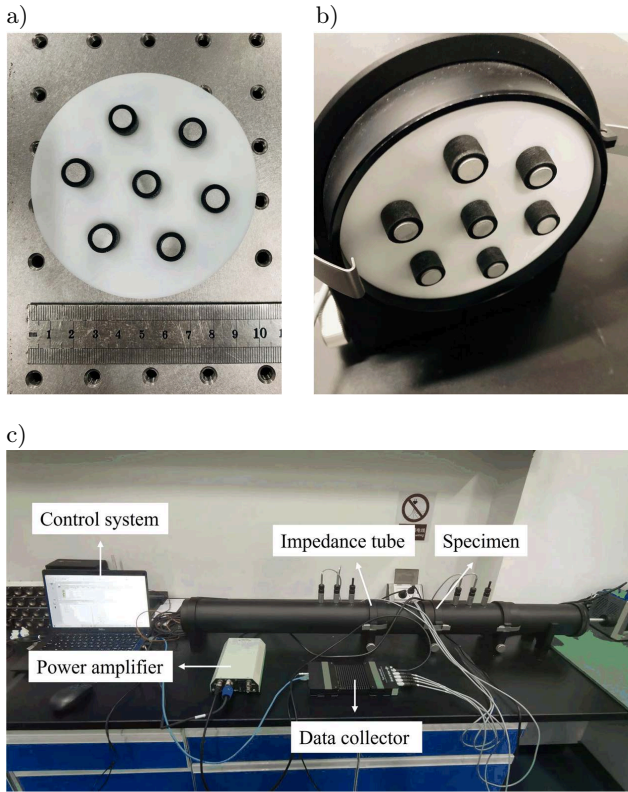


Fig. 1. Circular acoustic metamaterial samples (a); placement of the specimens in the experiment (b); sound insulation experimental test systems (c).

computer (installed with B&K acoustic test software) and impedance tube and other equipment (Fig. 1c). The impedance tube is 100 mm in diameter and consists of a large standing wave tube (including a loudspeaker and sample holder), a sample tube (for 0–100 mm wide samples), and a receiver tube. The test procedure is as follows: firstly, the relevant components of the impedance tube test system are installed and fixed in accordance with the requirements, ensuring that the whole impedance tube is on a horizontal line. Then, the B&K Acoustic Test Software is started and opened, and the relevant settings for the sound insulation items are set up. After no warnings have been given for the signal-noise ratio measurement, the sample tube is opened and the sample is placed into it, keeping the sample in a vertical plane as far as possible. Then, the sound insulation test is conducted and the sound insulation of the specimen can be obtained by substituting the sound pressure value into the transfer function.

### 2.2. Finite element simulation methods

In engineering practice, the sound insulation performance of structures is generally evaluated by sound transmission loss (STL). Noise reduction materials utilize various components, structures, or systems to hinder the spread of sound and diminish its energy once

it has passed through the material. To elucidate the sound insulation properties, the STL of the plate-type acoustic metamaterials is calculated.

In the  $x-z$  plane, there is an infinite homogeneous thin plate with thickness  $h$ , the top and bottom of which are in contact with the air, the speed of sound in the air is  $c$ , and the density of the air is  $\rho_0$  (Fig. 2). There is a simple harmonic plane wave  $P_{\text{inc}}$  incident from the  $z$  side, with acoustic wave amplitude  $P_0$ , incident angle  $\theta$ ,  $\omega$  is the incident angular frequency, and the wave vector of the incident wave  $k_0 = \omega/c$ . By decomposing  $k_0$  into two-dimensional coordinates, the projected components in the  $x$  and  $z$  squares are, respectively,  $k_x$  and  $k_z$ . According to Eq. (1), it can be observed that the plate vibrates under acoustic excitation, and the surface couples with the air to emit transmitted acoustic wave  $P_{\text{tr}}$  and reflected acoustic wave outward  $P_{\text{ref}}$ :

$$\begin{aligned} k_x &= k_0 \sin \theta, \\ k_z &= k_0 \cos \theta. \end{aligned} \tag{1}$$

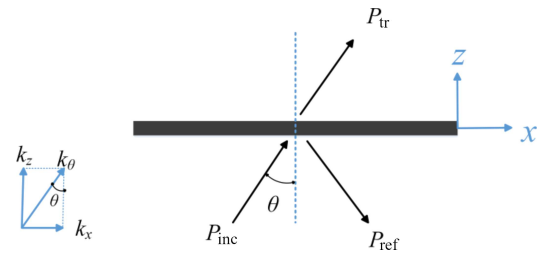


Fig. 2. Infinite homogeneous thin plate in the  $x-z$  plane.

According to the small amplitude one-dimensional plane wave equation  $P_{\text{inc}}$  can be assumed as:

$$P_{\text{inc}} = P_{i0} e^{-i(k_x x + k_z z)} e^{i\omega t} e^{i\varphi_0}, \tag{2}$$

where  $P_{i0}$  is the incident wave amplitude and  $\varphi_0$  is the initial phase of the incident wave at  $t = 0$ . Similarly, the reflected wave  $P_{\text{ref}}$ , transmitted wave  $P_{\text{tr}}$  and plate displacement  $w$  can be obtained as:

$$\begin{aligned} P_{\text{ref}} &= P_{r0} e^{-i(k_x x - k_z z)} e^{i\omega t} e^{i\varphi}, \\ P_{\text{tr}} &= P_{t0} e^{-i(k_x x + k_z z)} e^{i\omega t} e^{i\varphi}, \\ w &= W_0 e^{-ik_x x} e^{i\omega t} e^{i\varphi}. \end{aligned} \tag{3}$$

The equation of motion for an ideal fluid medium leads to Eq. (4):

$$\frac{\partial p}{\partial z} = -\rho_0 \frac{\partial v}{\partial t} = -\rho_0 \frac{\partial^2 w}{\partial t^2}. \tag{4}$$

According to the bending equation of a homogeneous thin plate, it can be obtained as:

$$\begin{aligned} D \frac{\partial^4 w}{\partial x^4} - \rho h \omega^2 w &= P_{\text{inc}}|_{z=0} + P_{\text{ref}}|_{z=0} - P_{\text{tr}}|_{z=0}, \\ D &= \frac{Eh^3}{12(1-\gamma)}, \end{aligned} \tag{5}$$

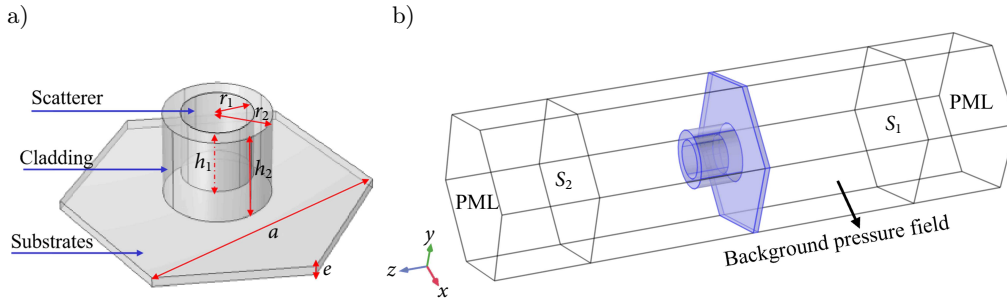


Fig. 3. Schematic illustrations of the unit cells of the plate-type acoustic metamaterial models (a) and schematic illustration of the calculation of the STL (b).

where  $E$  is Young's modulus of the plate material,  $D$  is the bending stiffness of the plate, and  $\gamma$  is Poisson's ratio.

Through Eqs. (2)–(4), the relationship between acoustic amplitude and plate amplitude can be obtained as:

$$\begin{aligned} P_{r0} - P_{i0} &= -\frac{\rho_0 i \omega^2 W_0}{k_z}, \\ P_{t0} &= \frac{\rho_0 i \omega^2 W_0}{k_z}. \end{aligned} \quad (6)$$

Then, substituting Eq. (6) into Eq. (5) to obtain  $P_{i0}$  as:

$$P_{i0} = \frac{W_0 \left[ D (k_0 \sin \theta)^4 - \rho h \omega^2 \right]}{2} + \frac{\rho_0 i \omega^2 W_0}{k_0 \cos \theta}. \quad (7)$$

The acoustic transmission coefficient  $\tau$  and the STL can be obtained as:

$$\begin{aligned} \tau(\theta) &= \frac{|P_{t0}|^2 / 2\rho_0 c}{|P_{i0}|^2 / 2\rho_0 c} \\ &= \frac{2\rho_0 i \omega^2}{\left[ D (k_0 \sin \theta)^4 - \rho h \omega^2 \right] k_0 \cos \theta + 2\rho_0 i \omega^2}, \end{aligned} \quad (8)$$

$$\text{STL}_{(\theta)} = 10 \log_{10} \left( \frac{1}{\tau(\theta)} \right). \quad (9)$$

An acoustic metamaterial type plate cell model was developed in COMSOL Multiphysics software (Fig. 3a). The basic parameters of the cell are: substrate thickness  $e = 1$  mm, and individual cell lattice constant  $a = 30$  mm. The radius and height of the cladding panel are  $r_2 = 6$  mm and  $h_2 = 9$  mm. In addition, the radius and height of the scatterer vary depending on the research scenario. Based on the acoustic metamaterial cell, we conducted an acoustic isolation simulation (Fig. 3b). The acoustic metamaterial type plate cell under study is shown in dark color at the center. There are two layers of air domains above and below the monocell. The uppermost layer serves as a perfect matching layer to absorb sound waves and simulate a non-reflective sound field. The lower air domain

of the wall plate is set as the background pressure field for acoustic excitation. The simulation uses acoustic-structure interaction and applies the perfectly matched layer (PML) to the model. A background pressure field ( $P_0$ ) is applied on the back of the plate. In this study, Eq. (8) is expanded to apply to the sound insulation simulation model structure, i.e., Eq. (10):

$$\tau_\theta = \frac{F_{\text{in}}}{F_{\text{out}}}, \quad (10)$$

$$F_{\text{in}} = \int_{S_{\text{in}}} \frac{P_{\text{inc}}^2 \cos \theta}{2\rho_0 c} dS, \quad (11)$$

$$F_{\text{out}} = \int_{S_{\text{out}}} \frac{P_{\text{out}c}^2 \cos \theta}{2\rho_0 c} dS, \quad (12)$$

where  $F_{\text{in}}$  and  $F_{\text{out}}$  are the acoustic energies on the two surfaces  $S_1$  and  $S_2$ ,  $S_{\text{in}}$  and  $S_{\text{out}}$  are the areas of  $S_1$  and  $S_2$ , respectively,  $P_{\text{inc}}$  and  $P_{\text{out}c}$  are the sound pressures of  $S_1$  and  $S_2$ , respectively,  $\rho_0$  is the air density,  $c$  is the velocity of sound waves propagating in the air, and  $\theta$  is the pitch angle of sound waves incident on the sound waves. By combining Eq. (9) and Eq. (10), we can calculate the STL.

### 3. Results and discussion

#### 3.1. Sound insulation (simulation and experimental)

In order to verify the simulation results, we carried out comparative experiments on acoustic metamaterial plates with scatterer radius of 4 and 5 mm. The obtained comparison curves between experimental and simulation results are presented in Fig. 4.

It can be seen in Fig. 4a that certain inconsistencies exist between the outcomes obtained from the experimental analysis and the finite element simulation results at the peaks of the sound insulation curve. Specifically, the frequencies of the peaks are 288 and 309 Hz, with corresponding sound insulation values of 52 and 45 dB, respectively. However, at the valleys of the curve, both the experimental results and

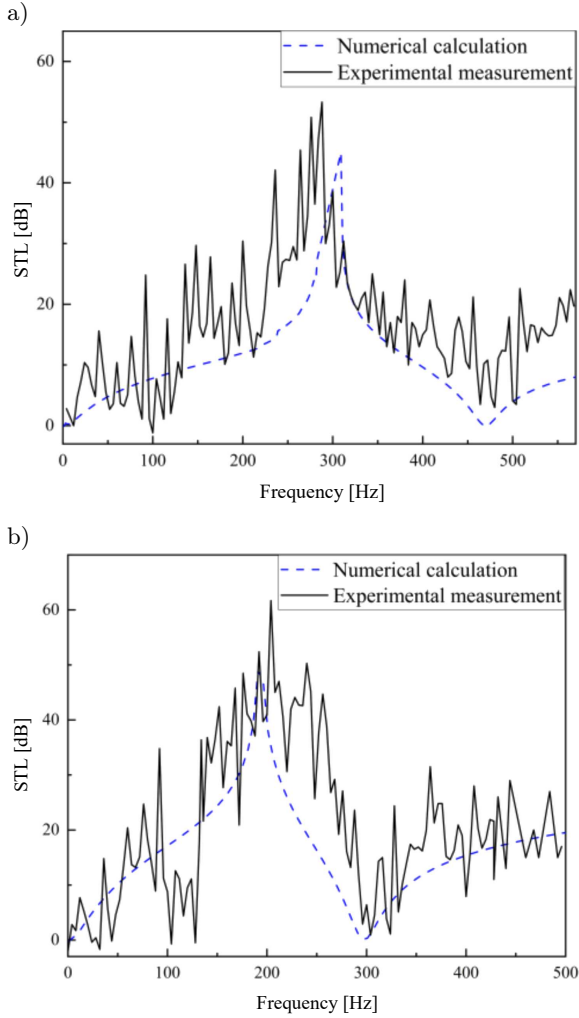


Fig. 4. Comparison curves between experiment and simulation for scatterer radius of 4 mm (a) and 5 mm (b).

finite element simulation results exhibit a consistent trend. The sound wave frequencies at these points are 475 and 463 Hz, with corresponding sound insulation values of 1 and 3 dB, respectively.

As can be seen from the curves in Fig. 4b, the growth or reduction trend of the sound insulation curves is basically consistent with the simulation curves. During the rising phase of sound insulation, the experimental results curve exhibits a faster growth than the simulation results curve, and there are some cliff-like decrease places, but the overall trend is still growing. The frequencies corresponding to the peaks of the experimental curves are slightly higher than the simulation results, with frequencies of the peaks of 209 and 198 Hz, and the corresponding sound insulation values of 61 and 49 dB, respectively. Additionally, the frequencies corresponding to the valleys of the experimental curves match the simulation results.

During the sound insulation experiment, errors in the measured sound insulation values and corresponding frequency bands may occur due to various factors

such as test equipment, sample processing, and the experimental environment. The specific reasons for the errors are: (1) the sound insulation values and corresponding frequency bands may have been affected due to limitations in the experimental equipment. This is because the actual tested specimen was a circular multi-cell specimen, which is different from the hexagonal single-cell specimen used in the simulation test; (2) the experimental measurements of sound insulation may vary due to potential errors in the manufacturing of the tested parts.

Overall, although there are some deviations between the experimental results and the simulation results, the finite element simulation results effectively predicts the sound insulation performance of acoustic metamaterial panels, and there is a certain reference significance in the overall trend of the sound insulation curve.

### 3.2. Limiting the total mass of the scatterers

We classify and discuss the effects of different scatterer radii (Fig. 5a) and sinking depth of the scatterer (Fig. 5b) on sound insulation, when the total mass of the limited scatterers is maintained constant, with the unit cell lattice constant  $a = 30$  mm, substrate thickness  $e = 1$  mm, and the cladding radius  $r_2 = 6$  mm, and the total height  $h_2 = 9$  mm kept unchanged.

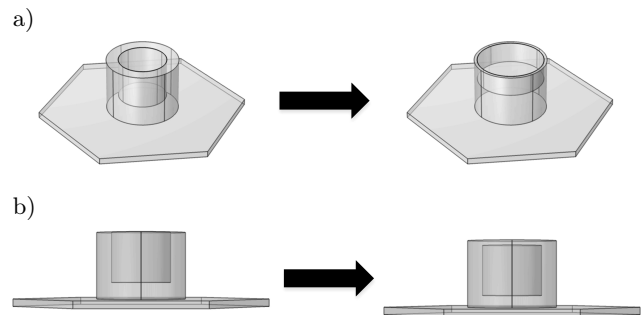


Fig. 5. The total mass of the scatterer is kept constant, changing the radius of the scatterer, with the height of the scatterer adjusting accordingly (a) and the radius and height of the scatterer remain unchanged, only the sinking depth  $Z$  of the scatterer is changed (b).

In order to quantify the advantages and disadvantages of different lattice constants, the effective sound insulation band is defined here as the band range in which the sound insulation is 5 dB higher than that of a homogeneous plate with the same mass (ZHANG *et al.*, 2016b). Therefore, we choose a range of sound insulation higher than 30 dB. The red dots marked as  $f_1$  and  $f_2$  represent the start and cut-off frequencies when the sound insulation is 30 dB (Figs. 6a and 6b). The normalization is calculated using Eq. (13):

$$\Delta f = \frac{f_2 - f_1}{(f_2 + f_1)/2}. \quad (13)$$

First of all, with the total mass of the scatterer held constant and only changing the radius of the scatterer, the height of the scatterer adjusts accordingly. We choose the radius  $r_1$  of the scatterer as 4, 4.5, 5, 5.5 mm, respectively, and the height  $h_1$  corresponds to 4.75, 5.3, 4.32, 3.57 mm. It can be clearly seen that the effective sound insulation band gradually shifts to the low frequency with an increase scatterer radius, the onset

of the effective sound insulation band gradually shifts to the low frequency with an increase scatterer radius, the onset

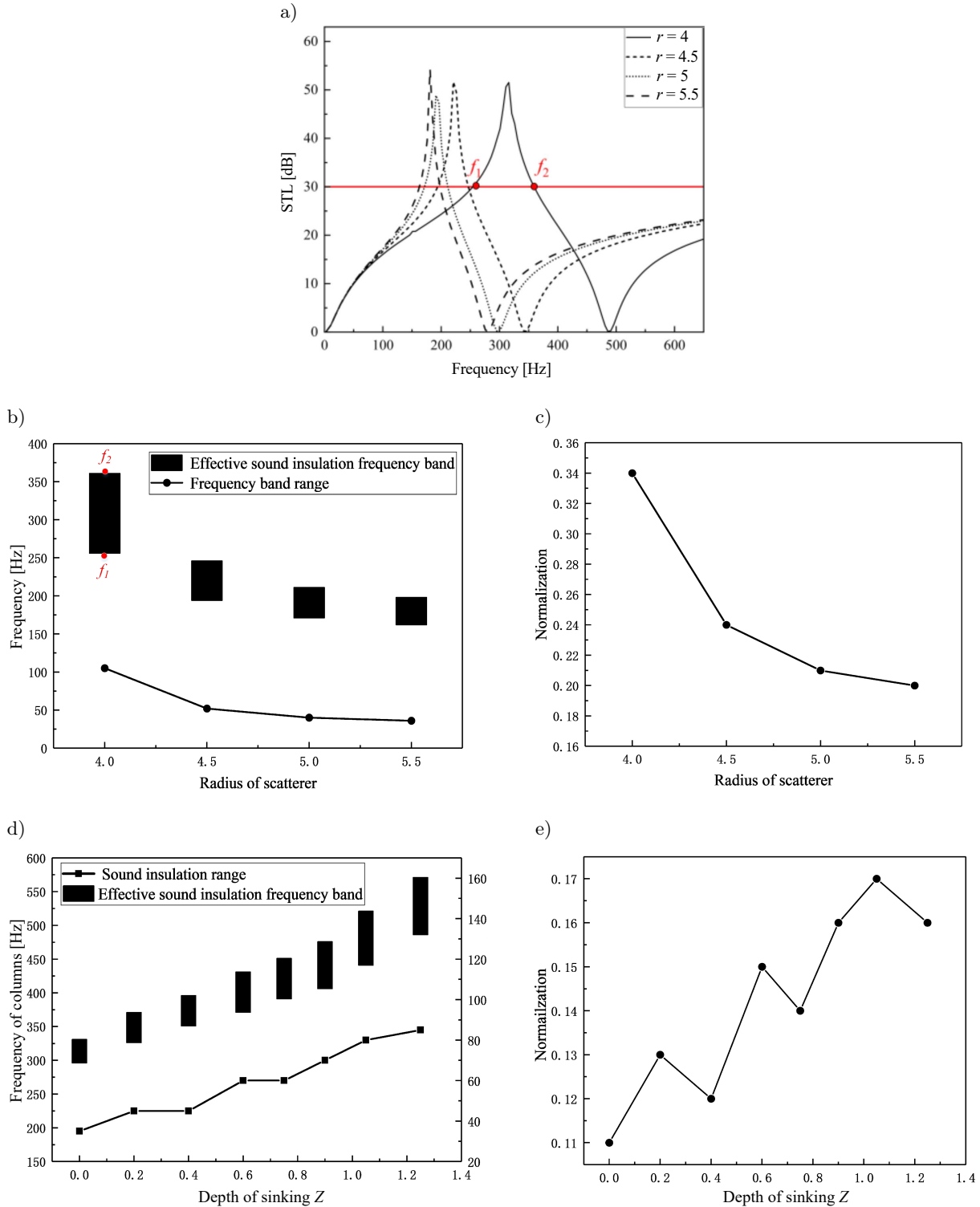


Fig. 6. a) Sound insulation curves corresponding to scatterers with radius of 4, 4.5, 5, and 5.5 mm; b) effective sound insulation frequency band and frequency band range corresponding to different scatterer radius; c) normalization curve for different scatterer radius; d) effective sound insulation frequency band and frequency band range of different sinking depth  $Z$  of scatterers; e) normalization curve for different sinking depth.

frequency decreases from 255 to 163 Hz, the cutoff frequency decreases from 363 to 198 Hz, and the sound insulation range decreases from 108 to 35 Hz (Fig. 6b). It is shown that the normalization is 0.34 when the radius of the scatterer is 4 mm, but it decreases to 0.2 when the radius increases to 5.5 mm (Fig. 6c).

Then, keeping the scatterer radius  $r_1 = 4$  mm and height  $h_1 = 6$  mm unchanged, the scatterer sinking depth  $Z$  is changed. Here,  $Z$  represents the distance between the upper surface of the scatterer and the upper surface of the cladding, with the selection range of 0~1.2 mm. The substrate material is aluminum, the cladding material is silicone rubber, and the diffuser material is copper (Table 1). As the sinking depth  $Z$  increases, the upper and lower limits of the effective sound absorption frequency band shift to high frequencies, and the frequency range gradually increases from 35 to 85 Hz (Fig. 6d). As the sinking depth increases, the normalization shows a stepwise growth trend, from 0.11 to 0.17, and then reaches a maximum of 0.17 at a sinking depth of  $Z = 1$  mm (Fig. 6e).

In summary, when limiting the additional mass of the resonance unit, the smaller the radius of the scatterer or the deeper the sinking depth  $Z$ , the closer the center of gravity of the scatterer is to the substrate, and the resonance unit as a whole is more stable. The range of effective sound insulation frequency band is obviously widened, and the frequency band is gradually shifted to high frequency, and the degree of normalization is also gradually increased. The band gap can be maximally broadened, and the sound insulation at low frequencies below 600 Hz can be realized, thus improving the low-frequency sound insulation efficiency of acoustic metamaterials.

### 3.3. Not limited to additional mass of the resonance unit

We classify and discuss the effects of different filling rates  $f$  and different materials of different components on sound insulation, when there are no restrictions on the additional mass of the resonance unit, with a cell constant  $a = 30$  mm, substrate thickness  $e = 1$  mm, the radius and height of the cladding are  $r_2 = 6$  mm,  $h_2 = 9$  mm and, additionally, the radius and height of the scatterer vary depending on the research scenario.

Initially, while maintaining the materials for the substrate, cladding and scatterer as aluminum, silicon rubber and copper, respectively, we consider a filling rate range from 0.3 to 0.6. The filling rate  $f$  is calculated from Eq. (7):

$$f = \frac{V_S}{V_C}, \tag{14}$$

where  $V_S$  and  $V_C$  are the volumes of the scatterer and the cladding, respectively. Then, with a constant filling

rate of 0.5, the materials of the scatterer and the substrate are changed. The scatterer materials are tungsten, lead, copper and steel, and the substrate materials are aluminum and epoxy resin (Table 1).

The effective sound insulation frequency band, corresponding to different filling rates  $f$ , shows an overall trend of increasing and then decreasing. When the filling rates is in the range of 0.3 to 0.5, the sound insulation range increases from 46 to 155 Hz, and the effective sound insulation frequency band gradually shifts to the high frequency. The cutoff frequency also increases from 252 to 436 Hz. As the filling rates increases from 0.5 to 0.6, the sound insulation range decreases and eventually settles at 107 Hz. However, the sound insulation range remains 27 Hz higher than at the filling rates of 0.4. This shows that the sound insulation effect is better when the filling rate is in the range of 0.45~0.6, and the sound insulation effect is best when the filling rate is 0.5 (Fig. 7a). As the filling rates increase, the normalization shows a trend of first increasing and then remaining stable, indicating that the filling rate is more stable in the range of 0.4~0.6, and the filling rates selected in this range are preferable in practical applications (Fig. 7b).

When the substrate is aluminum, increasing the density of the scatterer material causes a gradual decrease in the upper and lower boundary frequencies of the effective sound insulation band. However, when the substrate is epoxy resin, increasing the density of the scatterer material results in the upper and lower boundary frequencies of the effective sound insulation band shifting towards higher and lower frequencies, respectively (Fig. 7c). The scatterer material is arranged in the following order: steel, copper, lead, and tungsten, with a gradual increase in density from 7780 to 19 100 kg/m<sup>3</sup>. Regardless of whether the substrate material is aluminum or epoxy resin, the frequency band range and normalization both exhibit an increasing trend. However, when the substrate material is epoxy resin, the advantages are more obvious, resulting in a larger frequency band range and normalization compared to aluminum as substrate material (Fig. 7d).

The scatterer acts like the mass in a spring-mass oscillator. The density of the scatterers directly affects the total equivalent mass of the cylinder. A denser scatterer not only increases the unit weight of the acoustic metamaterial, but also increases the resulting bandgap of frequencies. Therefore, when selecting scatterers, it is recommended to use high-density and high-elastic modulus metals such as lead and tungsten to obtain a wider bandgap range. However, it is important to consider the impact of the quality factor in practical applications, making metals such as copper and steel viable choices as scatterers. Additionally, low density materials such as epoxy resins should be chosen as substrates when constructing phononic crystals.

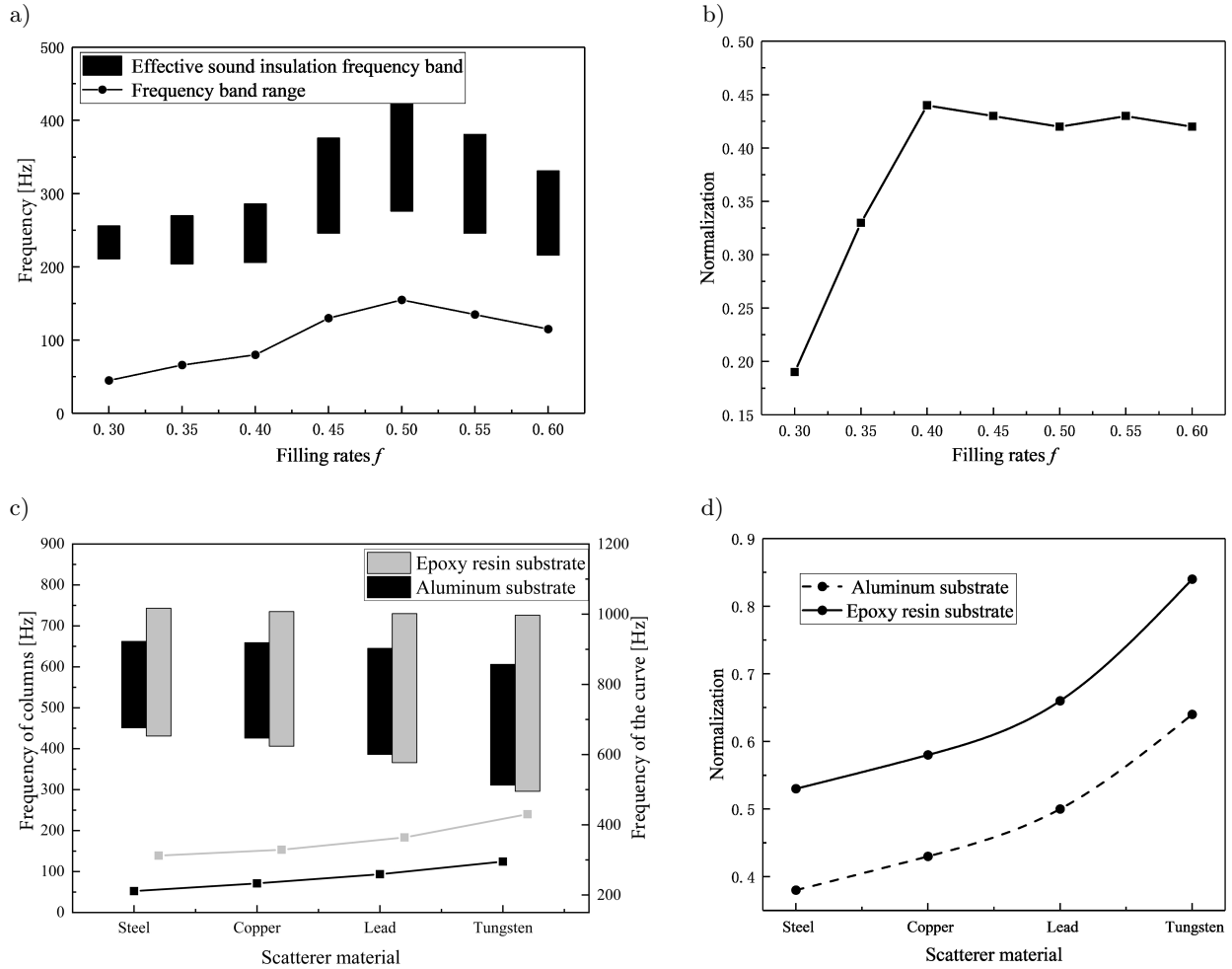


Fig. 7. a) Effective sound insulation frequency band and frequency band range corresponding to different filling rates; b) normalization curve for different filling rates; c) bar chart representing the effective sound insulation band and the curve representing the band range – the black color corresponds to the aluminum substrate and the grey color to the epoxy resin substrate; d) normalization curve for different materials.

#### 4. Conclusion

This paper proposed a plate-type acoustic metamaterial with good sound insulation in low-frequency ranges. In the study, we used finite element simulation to analyze the sound insulation characteristics of the three-component cladding acoustic metamaterial panel, and carried out experimental verification. The results show that the three-component cladding acoustic metamaterial plate can significantly suppress the propagation of noise across a wide frequency band below 600 Hz. Both theoretical and experimental findings demonstrate that the acoustic metamaterial plate provide excellent sound insulation, particularly at the resonant frequency of the local resonance unit. The effects of structural parameters of the scatterer, the filling rate of the resonant unit, and the materials of the components on the sound insulation properties of the acoustic metamaterials were subsequently investigated. The following conclusions are obtained.

When limiting the additional mass of the resonance unit, the smaller the radius of the scatterer or the deeper the sinking depth, the effective sound insulation frequency band shifts to high frequencies, and the frequency band range and normalization tend to increase. When the additional mass of the resonance unit is not limited, as the filling rate  $f$  increases, the effective sound insulation frequency band and frequency band range first increase and then decrease. Therefore, in order to obtain a better sound insulation effect, the filling rate should be kept at around 0.5. When selecting scatterer materials, it is recommended to use metals with high density and high-elastic modulus to obtain a wider bandgap range. Additionally, it is advisable to opt for a substrate material with a lower density.

#### Acknowledgments

This work was supported by the National Natural Science Foundation of China (U2033209).

*Data availability*

The data and programs that support the findings of this study are available from the corresponding author upon reasonable request.

*Conflicts of interest*

The authors declare that they have no conflicts of interest to report regarding the present study.

## References

1. ATMOJO A.Y. *et al.* (2021), ANC Gen1: BBT3-BPPT 1st prototype of active noise control for vehicle cabin noise, [in:] *Journal of Physics: Conference Series*, **1951**(1): 012030, doi: [10.1088/1742-6596/1951/1/012030](https://doi.org/10.1088/1742-6596/1951/1/012030).
2. BADREDDINE ASSOUAR M., OUDICH M. (2012), Enlargement of a locally resonant sonic band gap by using double-sided stubbed phononic plates, *Applied Physics Letters*, **100**(12): 123506, doi: [10.1063/1.3696050](https://doi.org/10.1063/1.3696050).
3. BADREDDINE ASSOUAR M., SENESI M., OUDICH M., RUZZENE M., HOU Z. (2012), Broadband plate-type acoustic metamaterial for low-frequency sound attenuation, *Applied Physics Letters*, **101**(17): 173505, doi: [10.1063/1.4764072](https://doi.org/10.1063/1.4764072).
4. CHEN D., ZI H., LI Y., LI X. (2021), Low frequency ship vibration isolation using the band gap concept of sandwich plate-type elastic metastructures, *Ocean Engineering*, **235**: 109460, doi: [10.1016/j.oceaneng.2021.109460](https://doi.org/10.1016/j.oceaneng.2021.109460).
5. HE X.D., WEN J.H. (2018), Study on the effect of lattice constants on the sound insulation properties of acoustic metamaterial plates, *Noise and Vibration Control (S1)*, pp. 51–55.
6. HSU J.C. (2011), Local resonances-induced low-frequency band gaps in two-dimensional phononic crystal slabs with periodic stepped resonators, *Journal of Physics D: Applied Physics*, **44**(5): 055401, doi: [10.1088/0022-3727/44/5/055401](https://doi.org/10.1088/0022-3727/44/5/055401).
7. HSU J.C., WU T.T., HSU H.S. (2013), Measurement of frequency gaps and waveguiding in phononic plates with periodic stepped cylinders using pulsed laser generated ultrasound, *Journal of Applied Physics*, **113**(8): 083511, doi: [10.1063/1.4793491](https://doi.org/10.1063/1.4793491).
8. IANNAC G., CIABURRO G., TREMATERRA A. (2021), Metamaterials acoustic barrier, *Applied Acoustics*, **181**: 108172, doi: [10.1016/j.apacoust.2021.108172](https://doi.org/10.1016/j.apacoust.2021.108172).
9. JIANG C., MOREAU D., FISCHER J., DOOLAN C. (2021), Additively manufactured sound-absorbing porous structures for airfoil trailing-edge noise control, *Journal of Aerospace Engineering*, **34**(5): 04021068, doi: [10.1061/\(ASCE\)AS.1943-5525.0001317](https://doi.org/10.1061/(ASCE)AS.1943-5525.0001317).
10. LI S., CHEN T., WANG X., LI Y., CHEN W. (2016), Expansion of lower-frequency locally resonant band gaps using a double-sided stubbed composite phononic crystals plate with composite stubs, *Physics Letters A*, **380**(25–26): 2167–2172, doi: [10.1016/j.physleta.2016.03.027](https://doi.org/10.1016/j.physleta.2016.03.027).
11. LI Y., CHEN T., WANG X., XI Y., LIANG Q. (2015), Enlargement of locally resonant sonic band gap by using composite plate-type acoustic metamaterial, *Physics Letters A*, **379**(5): 412–416, doi: [10.1016/j.physleta.2014.11.028](https://doi.org/10.1016/j.physleta.2014.11.028).
12. LIANG B., YUAN B., CHENG J.C. (2009), Acoustic diode: Rectification of acoustic energy flux in one-dimensional systems, *Physical Review Letters*, **103**(10): 104301, doi: [10.1103/PhysRevLett.103.104301](https://doi.org/10.1103/PhysRevLett.103.104301).
13. MA C., SHAO C., WAN Q., WANG X., CHENG Y., LIU X. (2018), A locally-resonant phononic crystal for low-frequency vibration control of vehicle [in Chinese], *Journal of Applied Acoustics*, **37**(1): 152–158, doi: [10.11684/j.issn.1000-310X.2018.01.022](https://doi.org/10.11684/j.issn.1000-310X.2018.01.022).
14. MALDOVAN M. (2013), Sound and heat revolutions in phononics, *Nature*, **503**(7475): 209–217, doi: [10.1038/nature12608](https://doi.org/10.1038/nature12608).
15. NAKAYAMA M. *et al.* (2021), A practically designed acoustic metamaterial sheet with two-dimensional connection of local resonators for sound insulation applications, *Journal of Applied Physics*, **129**(10): 105106, doi: [10.1063/5.0041738](https://doi.org/10.1063/5.0041738).
16. OUDICH M. *et al.* (2011), Experimental evidence of locally resonant sonic band gap in two-dimensional phononic stubbed plates, *Physical Review B*, **84**(16): 165136, doi: [10.1103/PhysRevB.84.165136](https://doi.org/10.1103/PhysRevB.84.165136).
17. OUDICH M., LI Y., ASSOUAR B.M., HOU Z. (2010), A sonic band gap based on the locally resonant phononic plates with stubs, *New Journal of Physics*, **12**(8): 083049, doi: [10.1088/1367-2630/12/8/083049](https://doi.org/10.1088/1367-2630/12/8/083049).
18. PENNEC Y., DJAFARI-ROUHANI B., LARABI H., VASSEUR J.O., HLADKY-HENNION A.C. (2008), Low-frequency gaps in a phononic crystal constituted of cylindrical dots deposited on a thin homogeneous plate, *Physical Review B*, **78**(10): 104105, doi: [10.1103/PhysRevB.78.104105](https://doi.org/10.1103/PhysRevB.78.104105).
19. QIU C., LIU Z. (2006), Acoustic directional radiation and enhancement caused by band-edge states of two-dimensional phononic crystals, *Applied Physics Letters*, **89**(6): 063106, doi: [10.1063/1.2335975](https://doi.org/10.1063/1.2335975).
20. SONG Y.B., WEN J., YU D., WEN X. (2015), Suppression of vibration and noise radiation in a flexible floating raft system using periodic structures, *Journal of Vibration and Control*, **21**(2), 217–228, doi: [10.1177/1077546313488156](https://doi.org/10.1177/1077546313488156).
21. WEN J., WANG G., YU D., ZHAO H., LIU Y. (2005), Theoretical and experimental investigation of flexural wave propagation in straight beams with periodic structures: Application to a vibration isolation structure, *Journal of Applied Physics*, **97**(11): 114907, doi: [10.1063/1.1922068](https://doi.org/10.1063/1.1922068).

22. WEN J.H., WANG G., YU D.L., ZHAO H.G., LIU Y.Z. WEN X.S. (2008), Study on the vibration band gap and vibration attenuation property of phononic crystals, *Science in China Series E: Technological Sciences*, **51**: 85–99, doi: [10.1007/s11431-008-0008-x](https://doi.org/10.1007/s11431-008-0008-x).
23. YANG Q. *et al.* (2020), Simulations on the wide bandgap characteristics of a two-dimensional tapered scatterer phononic crystal slab at low frequency, *Physics Letters A*, **384**(35): 126885, doi: [10.1016/j.physleta.2020.126885](https://doi.org/10.1016/j.physleta.2020.126885).
24. YIN J. *et al.* (2022), Review on research progress of mechanical metamaterials and their applications on vibration and noise control [in Chinese], *Advance in Mechanics*, **52**(3): 508–586, doi: [10.6052/1000-0992-22-005](https://doi.org/10.6052/1000-0992-22-005).
25. YU K., CHEN T., WANG X. (2013), Band gaps in the low-frequency range based on the two-dimensional phononic crystal plates composed of rubber matrix with periodic steel stubs, *Physica B: Condensed Matter*, **416**: 12–16, doi: [10.1016/j.physb.2013.02.011](https://doi.org/10.1016/j.physb.2013.02.011).
26. ZHANG J., YAO H., DU J., ZHAO J., DONG Y., QI P. (2016a), Low frequency sound insulation characteristics of the locally resonant phononic crystals in the large aircraft cabin [in Chinese], *Journal of the Chinese Ceramic Society*, **44**(10): 1440–1445, doi: [10.14062/j.issn.0454-5648.2016.10.08](https://doi.org/10.14062/j.issn.0454-5648.2016.10.08).
27. ZHANG H., XIAO Y., WEN J., YU D., WEN X. (2016b), Ultra-thin smart acoustic metasurface for low-frequency sound insulation, *Applied Physics Letters*, **108**(14): 141902, doi: [10.1063/1.4945664](https://doi.org/10.1063/1.4945664).
28. ZHAO H. J., GUO H.W., GAO M.X., LIU R.Q., DENG Z.Q. (2016), Vibration band gaps in double-vibrator pillared phononic crystal plate, *Journal of Applied Physics*, **119**(1): 014903, doi: [10.1063/1.4939484](https://doi.org/10.1063/1.4939484).
29. ZHAO H.J., GUO H.W., LI B.Y., DENG Z.Q., LIU R.Q. (2015), Flexural vibration band gaps in a double-side phononic crystal plate, *Journal of Applied Physics*, **118**(4): 044906, doi: [10.1063/1.4927627](https://doi.org/10.1063/1.4927627).
30. ZHOU P., WAN S., WANG X., FU J., ZHU Y. (2021), A novel hybrid composite phononic crystal plate with multiple vibration band gaps at low frequencies, *Physica B: Condensed Matter*, **623**: 413366, doi: [10.1016/j.physb.2021.413366](https://doi.org/10.1016/j.physb.2021.413366).
31. ZHOU X., WANG L., QIN L., PENG F. (2020), Improving sound insulation in low frequencies by multiple band-gaps in plate-type acoustic metamaterials, *Journal of Physics and Chemistry of Solids*, **146**: 109606, doi: [10.1016/j.jpcs.2020.109606](https://doi.org/10.1016/j.jpcs.2020.109606).
32. ZUO K.C. (2016), Current status of research on aircraft cabin noise, *Journal of Aviation*, **37**(8): 2370–2384.